Available online at www.sciencedirect.com

SciVerse ScienceDirect

Procedia Engineering 50 (2012) 649 – 657

Procedia Engineering

www.elsevier.com/locate/procedia

International Conference on Advances Science and Contemporary Engineering 2012 (ICASCE 2012)

Influence of water-vapor on the isothermal oxidation behavior of aluminized AISI 1020 steel at elevated temperatures

Mohammad Badaruddin[a]*, Sugiyanto[a], Ahmad Suudi[a]

[a]*Mechanical Engineering Department, Lampung University, Jalan Prof. S. Brojonegoro No.1 Bandar Lampung 35144, Indonesia.*

Abstract

The oxidation behavior of hot-dip aluminized AISI 1020 steel was studied at temperatures 700, 750, and 800 °C in air and water-vapor at atmospheric pressure. The high temperature oxidation of the steel has been improved by the hot-dip aluminized steel and the oxidation kinetics accords with a parabolic law. The aluminized steels exhibit a very low oxidation on the kinetics rates at elevated temperatures in air. Whereas, the aluminized steels exposed to water-vapor oxidation show that the alumina layer (Al_2O_3) formed on the surface coating has less protection than in air atmosphere. The presence of water in the oxidant gasses atmospheres leads to the rapid growth of sporadic iron oxide nodules on the coating surface and the steel substrate. Therefore, the oxidation rate is increased resulting in substantial mass-gain with the temperature and time.

Keywords: Aluminized AISI 1020 steel; water-vapor oxidation; iron oxide nodules; alumina layer

1. Introduction

AISI 1020 steel is used for low and medium pressure fluid pipe such as boiler superheater tube, boiling water pipe. It is often manufactured in the seamless steel pipe. The water-vapor in air atmosphere has been found to noticeably increase the corrosion rate of steel [1]. Numerous studies about the effect of water-vapor on steel and its alloys at high-temperature oxidation show that water-vapor contributes greatly to the high-temperature oxidation [2–6].

* Corresponding author. Tel.: +62-721-3555519; fax: +62-721-704947.
E-mail address: mbruddin@unila.ac.id (M. Badaruddin).

1877-7058 © 2012 Elsevier B.V...Selection and peer-review under responsibility of Bin Nusantara University
doi:10.1016/j.proeng.2012.10.071

Aluminizing coating on the steel and its alloys is one of the key technology to improve both oxidation resistance and fatigue life [5–9]. Aluminizing is usually carried out by the hot-dip process in which the component to be coated is treated in an aluminum molten bath containing 10 wt.% Si [10]. The addition of high silicon content is intended to reduce the thickness of aluminum coating on the substrate [11]. In the hot-dip process using the Al–Si alloy molten bath, the reduction of the Fe_2Al_5 intermetallic layer thickness is due to the tendency of Si to occupy the vacancies of the intermetallic Fe_2Al_5 phase. The Fe_2Al_5 phase possesses 30% vacancies along the c-axis with (001) direction, which offers a rapid diffusion path to increase the growth rate of Fe_2Al_5 [12]. The aluminide layer is expected to protect the steel surface by continuous formation of protective Al_2O_3 layer during exposure at elevated temperatures [5,7,9].

The present study focuses on the determination of high-temperature oxidation of steel with aluminizing coating at 700–800 °C. These temperatures represent the higher limit of temperatures that may be experienced by a steel pipe in high temperature steam condition. Reaction rates, morphology of reaction products, and composition changes occurring in the aluminized steel, are examined to provide an insight into the oxidation mechanisms.

2. Experimental procedures

The substrates were cut into coupons with the sizes of 20 mm ×10 mm ×1 mm from the commercial AISI 1020 steel with composition (wt.%); 0.2C–0.5Mn–0.04P–0.05S and Fe–balance. Before hot dip aluminizing all the samples were cleaned by 5% NaOH and 10% H_3PO_4, and then coated by uniform Al welding flux. The Al−10wt.%Si alloy was melted in an alumina crucible and maintained at 700 °C. The specimens, fixed by a hook made of stainless steel wire. The up/down speed of the specimen elevator was 15 cm/min. After 16 s of exposure, they were pulled out and air-cooled to room temperature.

The oxidation tests were performed at 700, 750, and 800 °C for 49 h periods in air and in mixtures of air + H_2O-vapour (steam). The fraction of H_2O was controlled by passing air at 200 mL/min through water bath heated to a specified temperature so that the partial pressure of H_2O can be adjusted. The temperature of water was thermostatically controlled at 100 °C. From a saturated steam table, 100 °C gives a steam content of 1 atm vapor pressure. The samples were placed in the furnace hot zone and after a given isothermal oxidation time, specimens were taken out and cooled in air at room temperature. Each mass-gain data point for the oxidation kinetics was obtained from different specimens.

Only the aluminized steel specimens were characterized as following. Structure of scales and phase formation were identified by X-ray diffraction (XRD) using monochromatic Cu-Kα radiation at 40 kV and 100 mA in in the Bragg-Brentano configuration with scanning range of $20° \leq 2\theta \leq 90°$ and step wise by 0.05°. The surface morphology and cross-sections of the specimens were examined using scanning electron microscopy (SEM) with backscattered electron image (BEI) signals, and energy dispersive spectroscopy (EDS) using spectrum range of 0–20 keV for a live time of 50 s.

3. Results and discussion

3.1. Effect of water-vapor on the oxidation kinetics

Figures 1(a–c) show the mass-gain kinetics for the bare and the aluminized steel during isothermal oxidation at 700 to 800 °C in air and steam environment. The curves show that in the air environment the steel exhibits low oxidation rates. Oxidation rate at all temperatures obeys a parabolic law in air and steam. Aluminized steels exhibit a relatively low oxidation rate. Furthermore, the oxidation rates consistently increase with the treatment temperatures; see Fig. 1(a–c). In addition, for specimens exposed to air oxidation, the mass-gains are lower than that of all specimens exposed to steam.

In order to identify the kinetic law in the tested temperature range, a plot of mass-gain versus square root of time, *t*, is very useful to give the values for the rate constant in the parabolic regime. The kinetics rate was determined by plotting of Δm/A versus $t^{1/2}$ for evaluation. As an example, a parabolic plot of Δm versus $t^{1/2}$ at 750 °C is presented in Fig. 1d; the extracted value of the kinetic constant for the bare steel, $k_p = 1.99 \times 10^{-8}$ g^2 cm^{-4} s^{-1}, is three orders of magnitude higher than that for all aluminized steels with $k_p = 1.17 \times 10^{-11}$ g^2 cm^{-4} s^{-1} in steam, and four orders of magnitude higher than that for all aluminized steels with $k_p = 2.25 \times 10^{-12}$ g^2 cm^{-4} s^{-1} in air. This indicates that the aluminized steel after being oxidized in the atmosphere containing water-vapor for 49 h as shown in Fig. 1b results in excellent performance. The lowest rate constant is obviously obtained when the aluminized specimens were oxidized in air.

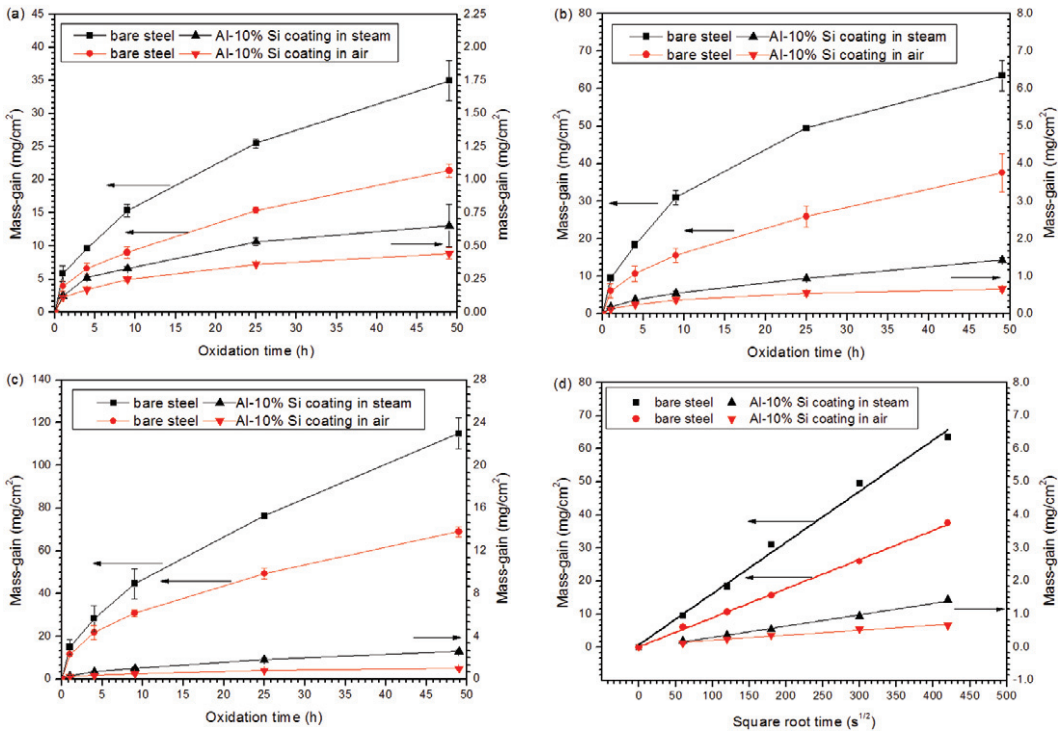

Fig. 1. Kinetics of bare steel and aluminized steel oxidized in different oxidizing gases at (a) 700 °C; (b) 750 °C; (c) 800 °C; (d) plot of parabolic kinetics for the specimens oxidized at 750 °C for 49 h.

There is a substantial mass-gain difference for specimens oxidized in both air and steam. Oxidation rates at 700, 750, and 800 °C for the aluminized steel in steam are higher rate due to the crack formation in the alumina scale and aluminide layer in presence of water-vapor, leading to the growth of sporadic iron oxide nodules. It is evident in Fig. 2 that local breakdown of the initial protective Al_2O_3 scale led to fast outward diffusion of Fe-ions resulting from the initial growth of nodules.

The fastest growth of nodules strongly give a contribution against the increase of mass-gains as result of the breakdown of the protective alumina layer (Al_2O_3). The coating layer fully lost its efficacy and, afterwards, oxidation could almost match the direct oxidation of the substrate steel. Cracking and growth of iron oxide nodules observed would be occurred in the coated specimen after high-temperature

oxidation. Thus, these limitations degrade the use of aluminized coatings for application in atmosphere containing water-vapour at high temperatures.

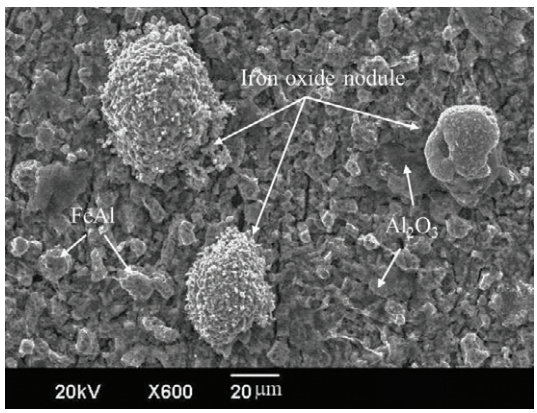

Fig. 2. SEM of surface morphology of the aluminized specimen exposed to steam at 700 °C for 49 h.

Figure 1c shows that the oxidation kinetics is faster at oxidation temperature of 800 °C. The oxidation rate constants (k_p) for the aluminized steel exposed to air and steam are about 4.84×10^{-12}, 4.07×10^{-11} g^2 cm^{-4} s^{-1}, respectively. The increase of oxidation rate is significant and strongly affected by the degradation of the protective Al_2O_3 layer. As reported by Sánchez et al. [4], the protective layer fails to protect alloys against an oxidant gas containing steam due to the consecutive degradation of the alumina in the Al depletion zone giving rise to the formation iron oxide nodule. The values for kinetics constants for the steel and aluminized steel exposed to both air and steam environment at temperature ranging from 700–800 °C for various duration of time from 1–49 h, are completely compiled in Table 1.

Table 1. The values of kinetics constants of bare steel and the aluminized steel exposed to air and steam environment

Environment	T (°C)	k_p (g^2 mg^{-4} s^{-1})	
		Bare steel	Aluminized steel
air	700	6.89×10^{-10}	8.70×10^{-13}
	750	7.72×10^{-9}	2.25×10^{-12}
	800	2.61×10^{-8}	4.84×10^{-12}
steam	700	6.92×10^{-9}	2.13×10^{-12}
	750	$1\,99 \times 10^{-8}$	1.17×10^{-11}
	800	7.40×10^{-8}	4.07×10^{-11}

3.2. Microstructure of as coated specimen

The SEM of cross-sectional micrograph of as coated specimen is shown in Fig. 3. According to EDS analysis, the coating surface to the interfacial zone consists of Al with Si-high dissolved, τ_5-Fe_2Al_8Si, $FeAl_3$ and finally Fe_2Al_5, see Fig. 3 (indicated by arrows). The formation of the polyhedral τ_5-Al_8Fe_2Si may be due to the monovariant peritectic reaction, $L + FeAl_3 \leftrightarrow \tau_5$-$Al_8Fe_2Si$ at 620 °C during cooling

from the diffusion temperature [10]. The large, polyhedral τ_5-Fe_2Al_8Si had a composition of 70.06Al–19.49Fe–10.45Si (at.%) and formed at the Al–Si /$FeAl_3$ layer. The confirmation of composition of the τ_5-Fe_2Al_8Si phase posed some problems as it was observed to show a wider composition range with Si and Fe concentrations varying from 9 to 13 at.% and 18 to 21 at.%, respectively. Silicon has a solubility of about 7.12 at.% in the $FeAl_3$ phase of this investigation, which is consistent within the range of about 1.06 to 7.12 at.% reported Maitra and Gupta [13]. The Fe-atoms substitution into $FeAl_3$ structure is similar to the Fe_3Al ordered structure [14]. The Si atoms were observed to replace Al atoms in all of the binary intermetallic of the Fe–Al system [13]. The intermetallic layer formed a distinctive serrated boundary with the substrate and was generally identified as Fe_2Al_5 with a composition of 66.91Al–21.75Fe–11.34Si (at.%). The high solubility of Si in the Fe_2Al_5 intermetallic contributed to generation of planar-like morphology toward to the steel substrate [12]. The overall coating thickness was around 27 μm, with a 4.2 μm thick intermetallic layer; the coating layer displayed good adhesion to the steel substrate.

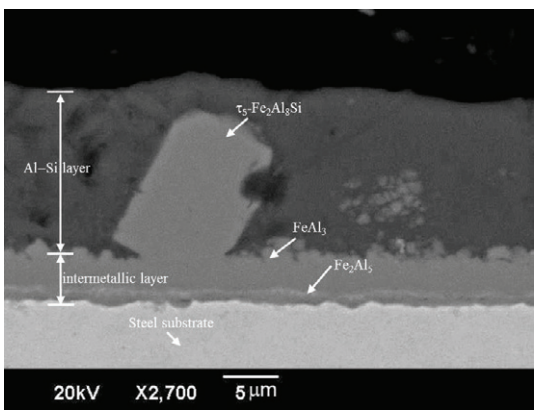

Fig. 3. SEM of cross-sectional micrograph of as coated specimen with EDS elements analyses.

3.3. Aluminide layer and X-Ray diffraction examinations after oxidation tests

The formation mechanism of the intermetallic compound during high temperature oxidation was dominated by inter-diffusion between Fe-atoms in the substrate and Al-atoms in the coating layer. After oxidation at temperature of 700 °C for 1 h, the τ_5-Al_8Fe_2Si and $FeAl_3$ layer of the as-coated specimen disappeared and transformed to Fe_2Al_5 and $FeAl_2$. The Si-high content in the $FeAl_3$ and τ_5-Fe_2Al_8Si layer had fast diluted in Fe-rich region due to the diffusion couple between diffusion inward Al atoms and outward diffusion Fe atoms, generating the bright particles of τ_1-$(Al,Si)_5Fe_3$ formed as precipitates in the Fe_2Al_5 and $FeAl_2$ phase of intermetallic layer (Fig. 4a). In addition, some voids formed and dispersed in the outer aluminide layer can be observed apparently in Fig. 4a. The change volume induced by phase transformation contributed to the void formation [10].

As oxidation time increase to 4 h and 9 h at 700 °C the τ_1-$(Al,Si)_5Fe_3$ phase transformed to form FeAl island in the outer aluminide layer, and FeAl island becomes to proportionally a greater size against the increase of diffusion time as shown in Fig. 4b. Some cracks were found in the aluminide layer due to the thermal expansion mismatch between the aluminide layer and the steel substrate [7], see Fig. 4c. The crack in the aluminide layer could later assist the transport of water-vapor to the oxidation reaction in the substrate and consequently enhanced the oxidation reaction by formation of iron oxide nodule. A continuous FeAl layer thickened gradually nearby the steel substrate because Fe-atoms diffused into

Fe_2Al_5 + $FeAl_2$ layer with increasing time owing to the aluminum dilution and the Fe_2Al_5 phase transformed subsequently to $FeAl_2$ (Fig. 4d). The Si solubility in both the FeAl islands and the continuous FeAl layer are similar in atomics composition of about 15–17% [13]. The thickness of aluminide layer consisting of a thin Al_2O_3 layer is kept almost the same with as coated specimen for all testing periods.

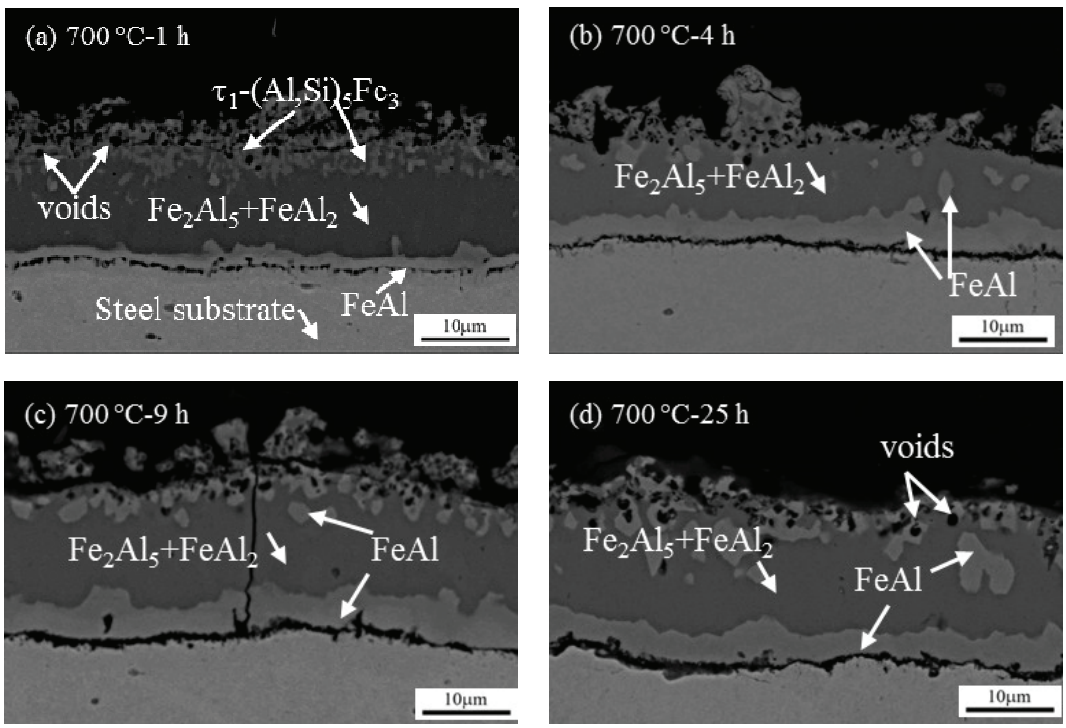

Fig. 4. BEI of cross-sectional micrograph of aluminized steel exposed to steam at 700 °C for (a) 1 h; (b) 4 h; (c) 9 h; (d) 25 h.

Iron-oxide nodule is clearly seen to form preferentially along surface crack direction in Fig. 5a. The SEM of surface morphology as shown in Fig. 5b reveals the morphology of the aluminized specimen after oxidation in air at 750 °C for 9 h; the surface morphology of rough aluminide layer consists of a protective Al_2O_3 layer. A protective coating should be dense and pore free in order to prevent the rapid oxidation of the steel substrate [15].

As mentioned above, the differences in absolute values of the oxidation rates of the aluminized steel in air and steam are related to the differences in relative amounts of Al-rich oxides in the outer surface scale. It should, however, be considered that in air-H_2O(g) mixtures competitive adsorption of oxygen and water-vapor molecules at external and internal surfaces of the oxide scale will affect the scale growth process. The experimental observations concerning the effect of water-vapor can be attributed by the suppression of protective alumina scale formation in high pressure of O_2 gases in the water-vapor. As reported by Taniguchi et.al [3], the diffusion of O_2-ions is faster than that Al-ions in the Al-rich zone is oxidized without its significant movement in the steam oxidation, and thus, the formation of thin Al_2O_3-rich layer is prevented. When the temperature oxidation is increased to 800 °C in steam, the result of XRD examination shows that peaks intensity for Al_2O_3 become lower than in air as shown in Fig. 6.

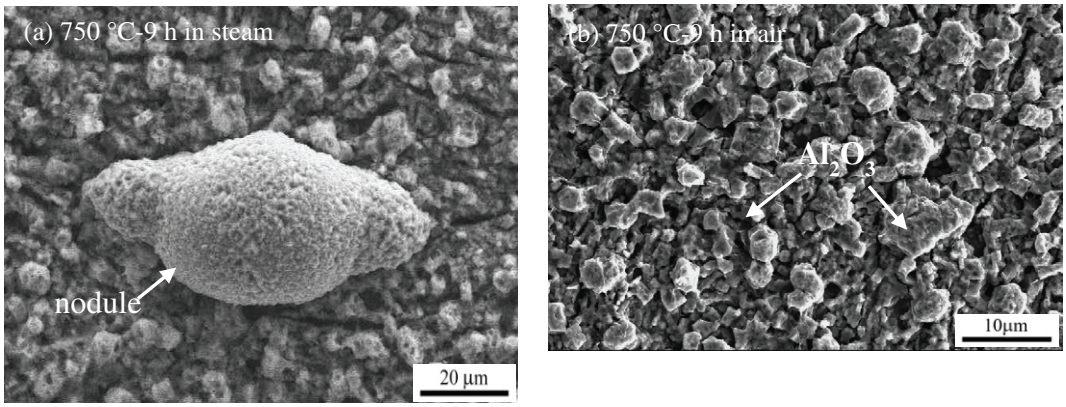

Fig. 5. SEM of surface morphology of aluminized steel oxidized at 750 ° C for 4 h (a) in steam; (b) in air.

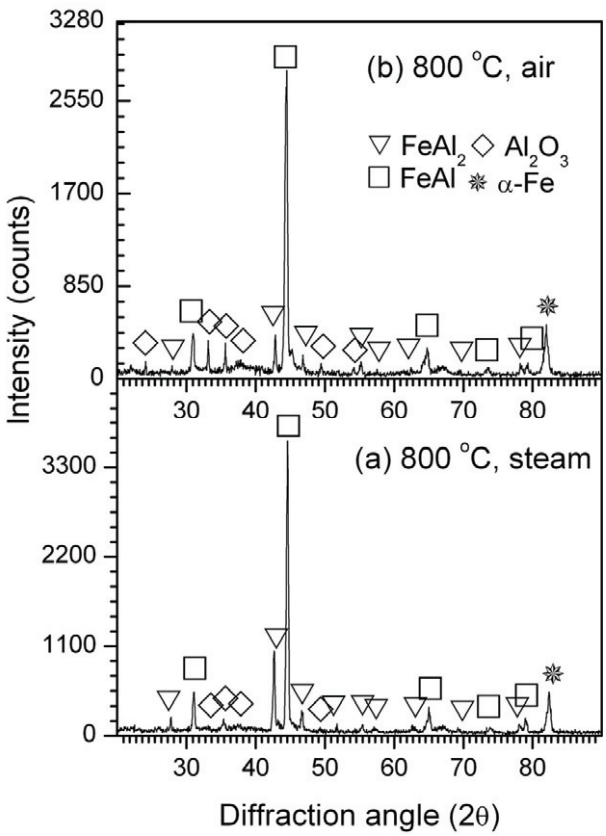

Fig. 6. XRD patterns of aluminized specimens after oxidation at 800 °C for 49 h.

As the temperature and exposure time increase, faster nodule growth destroys the protective Al_2O_3 scale. If iron-rich oxide nodules formation occurs via the outward diffusion of iron through the alumina layer via grain boundary diffusion, water vapor would be expected to accelerate this diffusion process. In

addition, the dissolution of hydrogen in iron oxide nodules also can increase the concentration of crystal defects by forming hydrogen defects in the oxide, and increase the rate of nodule growth. Therefore, the anisotropic diffusion of hydrogen was believed to have caused the directional growth of iron oxide nodules as shown in Fig. 2.

Figure 7a shows the mechanism by which water-vapor had access to transport process into the aluminide layer/substrate interface through crack path and H_2O directly oxidized the steel substrate, resulting rapidly in the formation of iron oxide nodule in the steel substrate after being oxidized at 800 °C for 49 h in steam. Observation of SEM of the cross-sectional image and EDS analysis in Fig. 7 show that the local formation of nodule on the alumina was not the result of excessive further Al depletion because about 54.06 at.% Al detected in regions of intact alumina is much more enough to maintain the supply of Al to growing alumina scale. Alternatively, the oxidation of initial stage of Al to form a continuous Al_2O_3 might be assisted by water vapor with the release of hydrogen at the early stage of oxidation [2,5]. The hydrogen dissolved into the alumina scale would generate the interstitial proton defects ($H_i^{\bullet}$). Furthermore, diffusion proton across the oxide layer generates increase in cation vacancies of Al^{3+}. Meanwhile, in Fe-rich zone, the iron will then take place as Fe^{2+} ions charges diffusing outward through the Al_2O_3 via aluminum vacancies. In addition, a high H_2 partial pressure resulted of hydrogen accumulation from H_2O dissociation, supports to alter oxygen-ions diffusion into the alumina scale and the further iron oxidation mechanism will locally more dominant in the formation of nodule. As the temperature increased and prolonged time, the faster growth of nodule will destroy the protective Al_2O_3 scale. Whereas, the formation of nodule at the interface aluminide layer/steel substrate was due to Al depleted to a lower concentration of 2.08 at.% Al, see Fig. 7b. Oxygen atoms diffused deeply to oxidize the steel substrate. Wide regions of Fe-rich oxide would suggest that O, rather than Al diffusion, is rate controlling in steel substrate, see Fig. 7a.

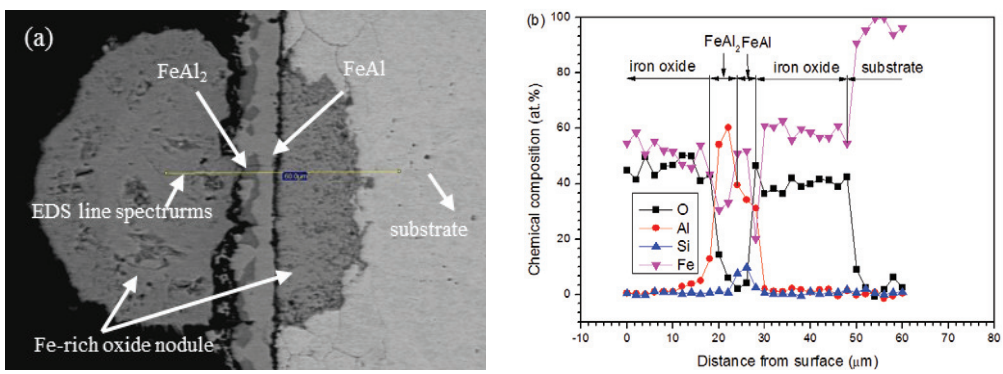

Fig. 7. (a) SEM of surface morphology; (b) EDS line profiles of chemical composition of aluminized steel oxidized at 800 °C for 49 h in steam.

4. Conclusion

The high temperature oxidation of AISI 1020 steel has been improved by the hot-dipping Al–10%Si coating at the temperature ranging from 700 to 800 °C for periods of 49 h in air and steam oxidation. The mass-gain of the aluminized steel increased with increasing of oxidation temperature and exposure time. The rate constant (k_p) of the aluminized steel exposed to steam is one order of magnitude greater than the aluminized steel exposed to dry air. The water-vapor in the atmosphere of oxidant gas did not affect the

phase transformation in formation of intermetallic compound of Al–Si–Fe. During phase transformation of aluminide layer induced defects/voids, the kinetics of oxidation observed in steam was accelerated by the presence of water-vapor. When water-vapor was present in the oxidizing gas mixtures the protective Al_2O_3 scale degraded to a greater extent than in air. The hydrogen produced by water-vapor dissociation at high temperatures dissolves in the alumina layer and later gives an increase in cation vacancies of Al^{3+} and consequently Fe-ions outwardly diffused, resulting in the formation of Fe-rich oxide nodules.

Acknowledgements

This research was financially supported by the Ministry of Research and Technology of Indonesia Republic via the incentive research of National Inovation System under contract No: 1.47/SEK/IRS/PPK/I/2012.

References

[1] Chen RY, Yuen WYD. Oxidation of low carbon steel in $17H_2O–N_2$ at 900 °C. *Metal Maters Trans A* 2009;**40A**:3091–17.

[2] Brady MP, Yamamoto Y, Santella ML, Walker LR. Composition, microstructure, and water vapor effects on internal/external oxidation of alumina-forming austenitic stainless steels. *Oxid Met* 2009;**72**:311–22.

[3] Taniguchi S, Hongawara N, Shibata T**.** Influence of water vapour on the isothermal oxidation behaviour of TiAl at high temperatures. *Mater Sci Eng A* 2001;**307**:107–5.

[4] Sánchez L, Bolívar FJ, Hierro MP, Pérez FJ. Temperature dependence of the oxide growth on aluminized 9–12%Cr ferritic-martensitic steels exposed to water vapour oxidation. *Thin Solid Films* 2009;**517**:3292–6.

[5] Wang CJ, Badaruddin M. The dependence of high temperature resistance of aluminized steel exposed to water-vapour oxidation. *Surf Coat Technol* 2010;**205:**1200–5.

[6] Badaruddin M, Wang CJ. Microstructure and high temperature oxidation of the hot-dipping Al-Si coating on low carbon steel in ethanol, water vapor and air at 700 °C. *Advanced Materials Research* 2009;**79-82**: 1775-4.

[7] Wang CJ, Chen SM. The high-temperature oxidation behavior of hot-dipping Al–Si coating on low carbon steel. *Surf Coat Technol* 2006;**200:**6601–4.

[8] Karel O, Simona P, Martin J, Tomas P, Jaroslav P. Effect of Al-Si diffusion coating on the fatigue behavior of cast Inconel 713LC. *Procedia Eng* 2010;**2**:1383–6.

[9] Badaruddin M. Improvement of high temperature oxidation of low carbon steel exposed to ethanol combustion product at 700 °C by hot-dip aluminizing coating. Makara Seri Teknologi 2011;**15(2)**:137–5.

[10] Cheng WJ, Wang CJ. Observation of high-temperature phase transformation in the Si-modified aluminide coating on mild steel using EBSD. *Mater Charact* 2010;**61**:467–6.

[11] Yousaf M, Iqbal J, Ajmal M. Variables affecting growth and morphology of the intermetallic layer (Fe_2Al_5). *Mater Charact* 2011;**62**:517-25.

[12] Cheng WJ, Wang CJ. Effect of Si on the formation of intermetallic phases in aluminide coating on mild steel. *Intermetallics* 2011;**19**:1455–5.

[13] Maitra T, Gupta SP. Intermetallic compound formation in Fe–Al–Si ternary system: Part II. *Mater Charact* 2003;**49**:293–8.

[14] Awan GH, Hasan FL. The morphology of coating/substrate interface in hot-dip-aluminized steels. *Mater Sci Eng A* 2008;**472**:157–8.

[15] Paldey S, Deevi SC. Cathodic arc deposited FeAl coatings: properties and oxidation characteristics. *Mater Sci Eng A* 2003;**355**:208–7.